ARTICLE

Self-Organization of a Discotic Coordination Complex Bearing Orthogonal Discotic Ligands

Nigel T. Lucas,[†] Hadi M. Zareie,[‡,*] and Andrew M. McDonagh[‡,*]

[†]School of Chemistry, The University of Sydney, NSW 2006, Australia, and [‡]Institute for Nanoscale Technology, University of Technology Sydney, P.O. Box 123, Broadway NSW 2007, Australia

ABSTRACT A new coordination complex that incorporates discotic ligands oriented orthogonally to a central discotic unit has been synthesized, and images of self-organized structures on highly oriented pyrolytic graphite have been obtained. Scanning tunneling microscopy images show that the combination of the orthogonally disposed discotic components results in significantly different self-organized structures compared to those of the ligand, which contains a single discotic unit.

KEYWORDS: hexa-*peri*-hexabenzocoronene · phthalocyanine · ruthenium · scanning tunneling microscopy

We present the synthesis of a new coordination complex that incorporates discotic ligands oriented orthogonally to a central discotic unit. Scanning tunneling microscopy (STM) data are presented that show the self-organized structures formed by the discotic ligand and the complex on highly ordered pyrolytic graphite (HOPG) surfaces.

Discotic molecules substituted with alkyl chains have been shown to self-organize into columnar mesophases.[1,2] The most intensively studied mesogens are based on triphenylenes, phthalocyanines, porphyrins, and, more recently, hexa-*peri*-hexabenzocoronenes (HBCs). The HBC mesogens consist of a rigid, planar polycyclic aromatic core of 42 carbon atoms, substituted with long alkyl chains at the periphery. Nanosegregation of the aromatic and alkyl components into one-dimensional columnar superstructures is stabilized by overlap of π-orbitals on adjacent molecules (π−π stacking). The interaction between adjacent aromatic cores provides a pathway for one-dimensional charge transport, a property that has attracted some attention.[3,4] HBC-based materials show relatively high charge-carrier mobilities, as determined by pulse radiolysis time-resolved microwave conductivity measurements and are considered strong candidates as semiconductor materials in field-effect transistors, photovoltaic cells, and light-emitting diodes.[5–7]

Thin films of HBCs with extremely long-range order have been prepared using solution techniques on glass[8] and treated silica[7] surfaces. The compounds used to form these structures typically have D_{6h} symmetry with symmetrical substitution about the periphery.

There are very few reports of the use of HBC compounds as ligands for coordination compounds.[9–13] Recent advances in synthetic techniques,[14] especially in the area of HBCs with unsymmetrical peripheral substitution, have enabled the preparation of HBC compounds with substituents that act as ligands in metal complexes.[10,11,13] In this report, we describe the synthesis of an HBC compound with an appended pyridine group, which is subsequently doubly coordinated to a ruthenium metal center in a phthalocyanine complex. This synthesis combines two archetypal discotic molecules in a mutually orthogonal geometry. STM experiments are used to probe the effect of molecular shape and disposition of the discotic units on the self-organized structures formed on graphite.

RESULTS AND DISCUSSION

Synthesis. Scheme 1 shows first the synthesis of the HBC-pyridine compound, **1**. A Suzuki-type coupling reaction[15] was used to couple 2-bromo-5,8,11,14,17-pentadodecylhexa-*peri*-hexabenzocoronene[16] with the pinacol ester of pyridine-4-boronic acid to give **1** in good yield.

The ^{1}H NMR spectrum of **1** contains signals in the range δ 2.98–0.90 assigned to the peripheral alkyl groups, and proton resonances associated with the pyridine group are observed as doublets at δ 8.85

*Address correspondence to hadi.zareie@uts.edu.au, andrew.mcdonagh@uts.edu.au.

Received for review May 7, 2007 and accepted October 11, 2007.

Published online November 30, 2007. 10.1021/nn700187b CCC: $37.00

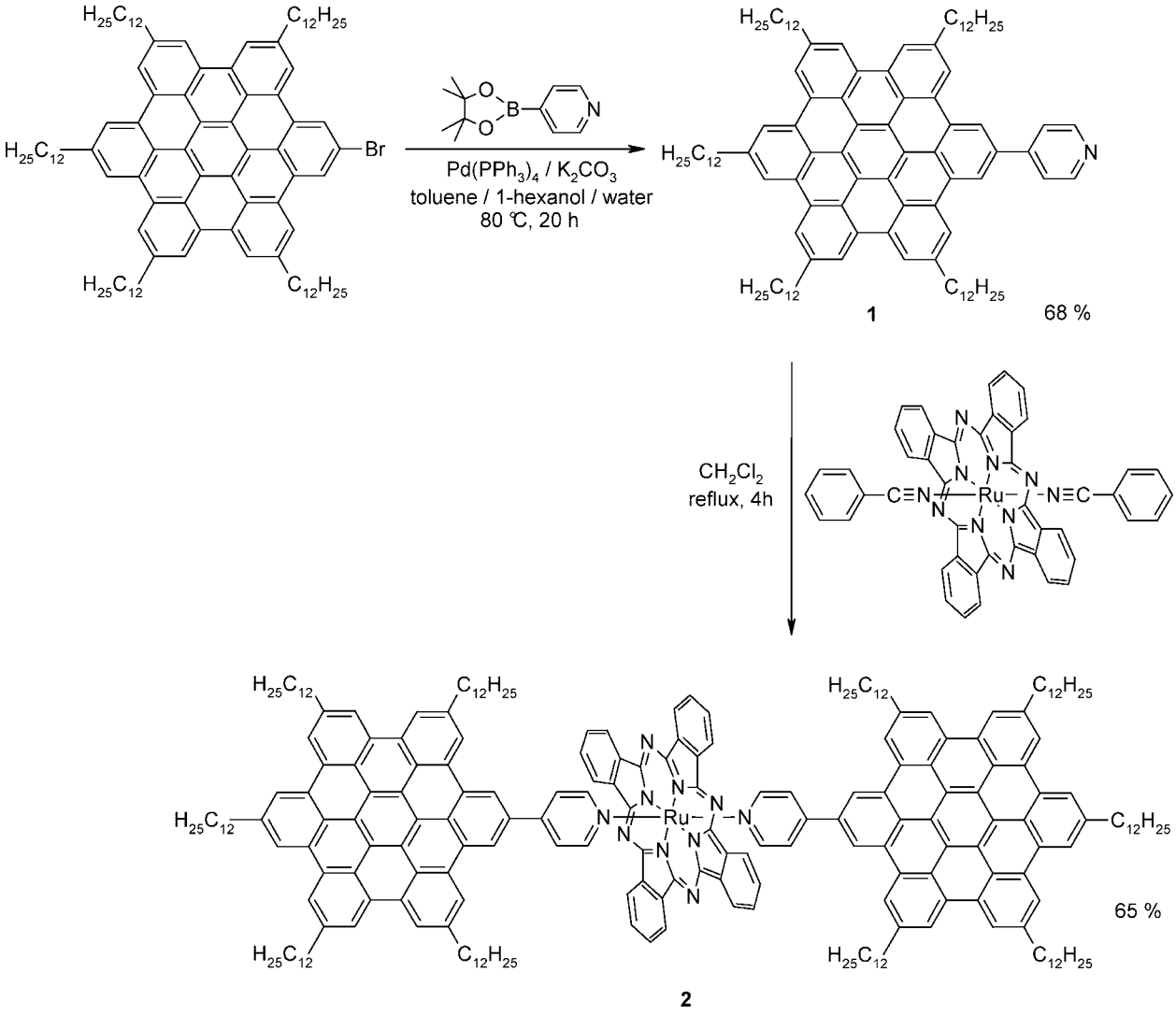

Scheme 1. Synthesis of 1 and 2.

and 7.57. Resonances assigned to the protons of the HBC core are observed as six broad singlets in the range δ 8.28–7.82. The mass spectrum of **1** shows the major signal as an envelope of peaks at $m/z = 1442$, with an isotope pattern matching that calculated for $C_{107}H_{141}N$.

The UV–visible spectrum of **1** is shown in Figure 1 (dotted trace). HBC compounds generally have three main electronic absorption bands. The weakest, the symmetry-forbidden α-band, appears at the lowest energy. This band has been assigned to a transition from the second highest occupied molecular orbital (HOMO-1) to the lowest unoccupied molecular orbital (LUMO).[17] The p-band occurs at intermediate energy and has been assigned to the HOMO–LUMO transition. The highest energy absorption, the β-band, is generally the most intense and has been assigned to a transition from the HOMO to the second lowest unoccupied orbital (LUMO+1).[18] In the spectrum of **1**, the α-band is observed as a series of peaks at 445, 449, and 470 nm, with a relatively low molar absorptivity (1560–3500 M^{-1} cm^{-1}). The relatively narrow p-band is observed at 395 nm, while the β-band comprises a series peaks between 316 and 365 nm, the latter being the most intense of the spectrum (118 800 M^{-1} cm^{-1}). Interestingly, the spectrum of **1** is similar to that of the symmetrically substituted 2,5,8,11,14,17-hexadodecylhexa-*peri*-hexabenzocoronene.[19] Müllen *et al.* recently showed that the alkyl substituents have virtually no effect upon the electronic spectra of HBC compounds,[18] and as observed here, substitution of one C_{12} chain

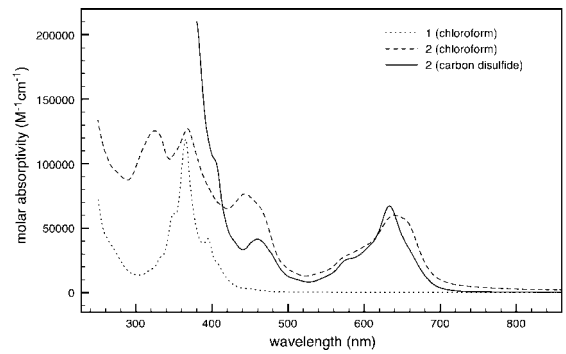

Figure 1. UV−visible spectra of 1 and 2.

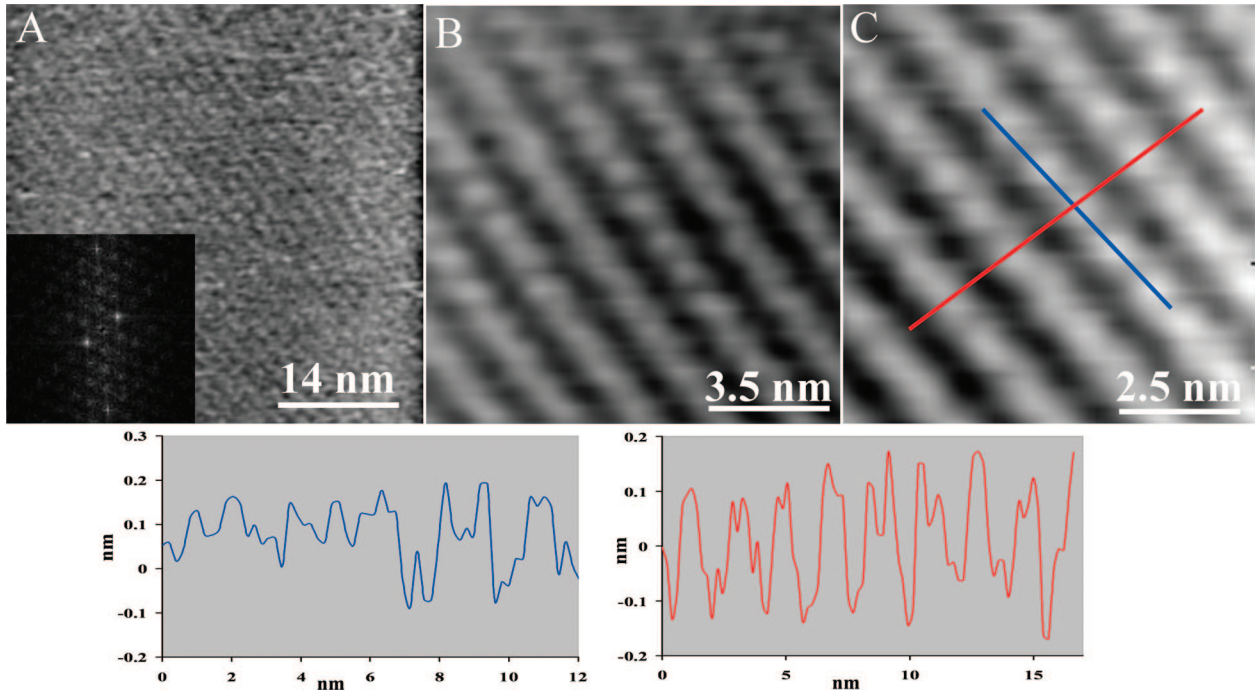

Figure 2. STM images of ordered assemblies of 1 on HOPG. Samples were prepared by applying a 1 mM solution of 1 onto HOPG substrates. (A) Large area image (inset: Fourier transform showing periodic pattern). (B) Magnified region from image A. (C) Image showing the regions used for line profile measurements. Images are raw data except for C, which is contrast-enhanced and low-pass-filtered to accentuate molecular features (using a SPIP Scanning Probe Image Processor[26]). Line profiles were obtained from raw data. STM images were recorded under constant-current mode with a 30 pA tunneling current and a −500 mV bias voltage (indicating the STM tip is negative with respect to the substrate). STM constant current mode images have been recorded using scan rates of 10–50 lines/s.

with pyridine also has little impact on the electronic spectrum.

The synthesis of the coordination complex **2** is also shown in Scheme 1. Replacement of the labile benzonitrile ligands of $[PcRu(NCPh)_2]$[20] with HBC-pyridine ligands afforded **2** in moderate yield. In contrast to the precursors, **2** exhibits low solubility in chlorinated solvents and requires the use of carbon disulfide mixtures to effect purification and solution characterization.

The ^{1}H NMR spectrum of **2** contains signals corresponding to the phthalocyanine ring protons at δ 9.32 and 8.02, and HBC core protons between δ 8.57 and 8.07 (broad singlets). The proton resonances of the coordinated pyridine groups appear at δ 6.02 and 2.91, significantly upfield compared to those of the uncoordinated ligand. The protons closest to the phthalocyanine experience the greatest shielding due to macrocyclic diamagnetic ring currents,[21] and thus the signal at δ 2.91 is assigned to the four protons adjacent to the pyridine N atoms. The signal at δ 6.02 is assigned to the pyridine protons adjacent to the HBC groups. The dodecyl groups of the axial ligands are observed as mostly broad multiplets in the range δ 3.04–0.89. Matrix-assisted laser desportion/ionization time-of-flight(MALDI-TOF) mass spectrometry shows the decomplexed ligand as the major species, the relatively weak Ru−N bonds precluding observation of a molecular ion under the range of conditions investigated.

The UV–visible spectrum of **2** is shown in Figure 1 (dashed and solid traces). The spectrum of **2** is similar to a superposition of a spectrum of a typical $[PcRu(py)_2]$ complex[22] (where py are pyridine or substituted pyridine ligands) and the spectrum of **1**. This suggests that there is little interaction between the HBC units of the axial ligands and the metal complex. Although this is consistent with the discotic axial ligands oriented in an orthogonal configuration relative to the plane of the central metallophthalocyanine discotic unit (*i.e.*, distorted octahedral coordination at Ru), molecular modeling studies were undertaken to confirm this geometry (see below).

Self-Organized Nanostructures on Graphite. Thin films of **1** and **2** were prepared by depositing solutions of **1** or **2** in toluene onto HOPG surfaces. After solvent evaporation, the samples were analyzed using a scanning tunneling microscope. Figure 2 shows STM images of **1** on HOPG. Ordered areas are observed where the HBC molecules align into rows. A similar structural arrangement has been previously reported for the symmetrical, peripherally substituted $HBC(C_{12}H_{25})_6$[7] and the lower symmetry pentaalkyl-substituted $HBC(C_{12}H_{25})_5$[16] compounds.

Line profile measurements (Figure 2) indicate an inter-row spacing of ~1.9 nm and an intra-row spacing of ~1.1 nm. The inter-row spacing is somewhat smaller than the spacing of 2.64 nm reported for structures of the symmetrical dodecyl-substituted

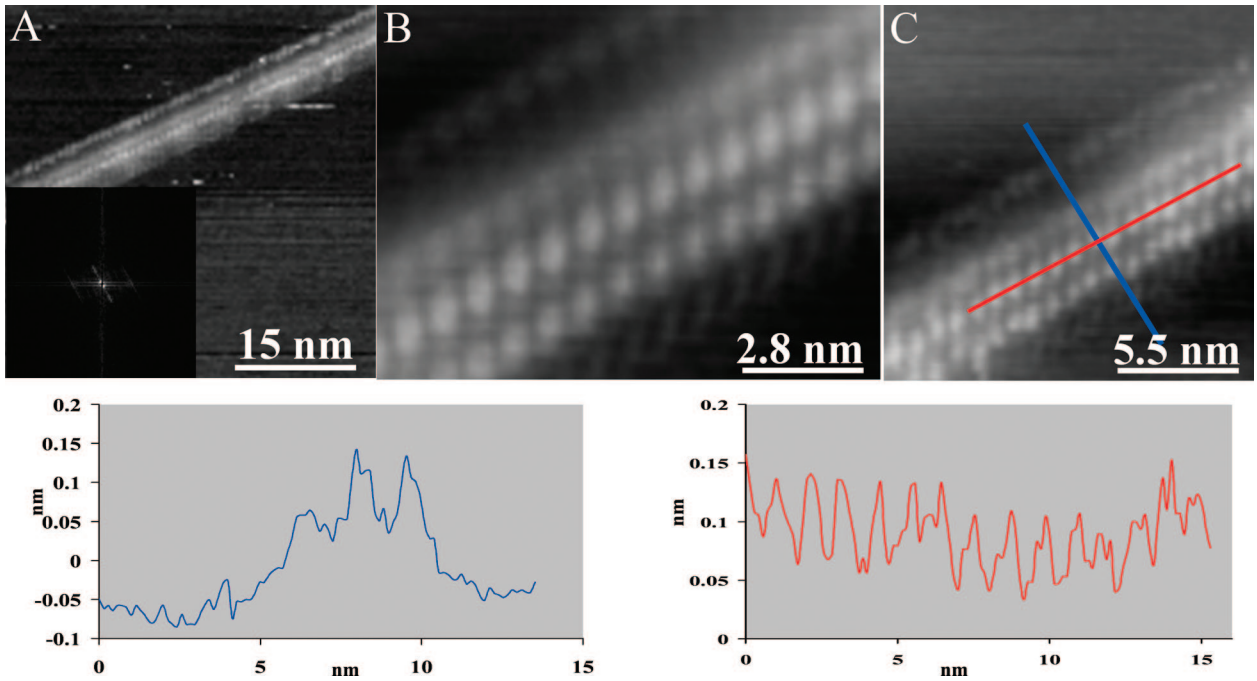

Figure 3. STM images of ordered assemblies of 2 on HOPG. Samples were prepared by applying a 1 mM solution of 2 onto HOPG substrate. (A) Large area image (inset: Fourier transform of large area image). (B) Higher magnification of A. (C) Line profiles of a section of A. Images are raw data except for B, which is contrast-enhanced and slightly low-pass-filtered to accentuate molecular features (using SPIP). The STM images were recorded under constant-current mode with a 6 pA tunneling current and a −700 mV bias voltage (indicating the STM tip is negative with respect to the substrate). STM current mode images were recorded using scan rate of 15 lines/s.

$HBC(C_{12}H_{25})_6$ compound on HOPG[19] and also the 2.48 nm spacing reported for $HBC(C_{12}H_{25})_6$ compound on silicon dioxide.[7] This suggests that there is a significant degree of overlap between substituents on molecules in adjacent rows, although we are unable to ascertain if this occurs between dodecyl or pyridine groups.

The intra-row spacing of ~1.1 nm is significantly less than the distance of 1.94 nm reported for structures of the symmetrical $HBC(C_{12}H_{25})_6$ compound on HOPG,[19] where the discs lie flat on the surface, but significantly larger than the value of 0.49 nm for $HBC(C_{12}H_{25})_6$ on silicon dioxide,[7] where the discs form tilted columnar arrangements with cofacial distances of 0.34 nm (which match the cofacial distance of 0.35 nm for bulk $HBC(C_{12}H_{25})_6$ from X-ray analysis).[23] The current data indicate that **1** does not lie flat on the graphite surface but also does not form edge-on columnar structures. Molecular modeling of **1** using Spartan[24] indicates a diameter of the HBC core of ~1 nm and an overall diameter including alkyl chains of ~3–4 nm. These data suggest the molecules are canted with respect to the surface. This is also indicated by the apparent molecular heights, as shown in the line profile data, where height variations between rows are significantly greater than those along a row. It should be emphasized, however, that STM investigations of thiol-bound SAMs on gold have found that heights measured by STM are not necessarily the same as the physical film thickness, as height data involve a convolution of electronic and physical properties.[25] We also note that, due to the dense packing, the apparent height does not necessarily match the height of the molecular layer with respect to the substrate, as the tip may be unable to probe the substrate between the rows.

Figure 3 shows STM images of **2** on HOPG. Within regions of the HOPG surface, molecules are aligned in structures that extend well over 100 nm. In contrast to the structures observed for **1**, there are no nearby rows. Line profile measurements are also shown in Figure 3. These data reveal that the width of the structures is ~7 nm, with an intra-row spacing of ~1 nm. Although a number of these structures could be observed in larger area images (see Supporting Information), we note that the solution casting preparation procedure used here will invariably give some regional inhomogeneity, as the gradient of concentration caused by the gradual evaporation of the solvent leads to various concentrations of molecules per surface area in a given sample. As a consequence, some areas of the surface contained regions where no ordering of the molecules was apparent.

The geometry of **2** was investigated computationally using the molecular mechanics method within the Spartan[24] program. The large number of atoms in the structure of **2** (257 non-hydrogen atoms, 298 hydrogen atoms) renders calculations at higher levels of theory somewhat demanding. The smaller model complex $[RuPc\{HBC(Me)_5\text{-}4\text{-}py\}_2]$ was investigated to ascertain the preferred disposition of the HBC-pyridine ligands relative the phthalocyanine unit. The minimum energy equilibrium geometry displays a planar metallophthalocyanine core with axial pyridine groups close to nor-

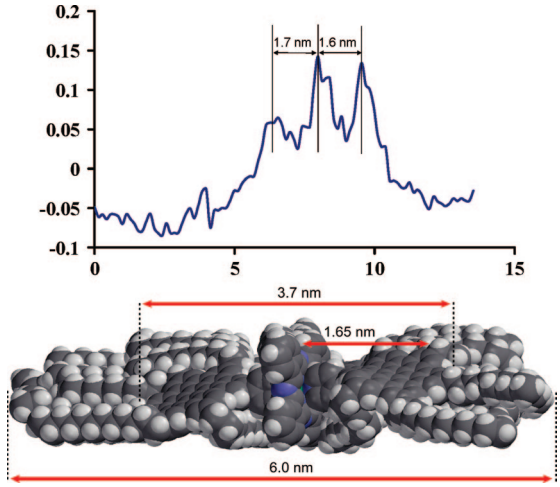

Figure 4. (A) Line profile data for structures of 2 on HOPG as indicated in Figure 3C (blue line). (B) Space-filling structural diagram and dimensions for 2 from Spartan calculations.

mal (N_{Pc}–Ru–N_{py} = 88.5–91.6°). The pyridine ligands are oriented ~45° relative to the Ru–Pc bond vectors, and a mutually orthogonal arrangement is marginally lower in energy than a coplanar arrangement. Interestingly, the plane of each pyridine intersects the Pc at the non-coordinating ring N atoms, similar to the geometry found in one of the few reported RuPc crystal structures.[27] Repulsion between the hydrogen atoms *ortho* to the HBC–py bond is reduced through an ~80° twist. The optimized geometry of **2** reveals that the ligands are oriented similarly to those in the [RuPc{HBC(Me)$_5$-4-py}$_2$] complex. A tip-to-tip length of **2** of ~6.0 nm and a distance of ~3.7 nm spanning the two HBC core extremities was calculated (see Figure 4). These distances closely match the experimental data obtained for **2** using STM. From this, we deduce that the structures such as those shown in Figure 3 consist of a single, isolated row of molecules of **2**.

Figure 5 shows a packing arrangement consistent with the experimental data supported by molecular mechanics calculations. As a consequence of the orthogonal disposition, the metallophthalocyanine sits edge-on to the surface, and the HBC ligands adopt canted orientations. We suggest that the brighter spots in the STM images correspond to the discotic units, while the fainter regions observed on either side of the brighter areas are attributed to the dodecyl chains. Line profile measurements indicate a distance of 1.6–1.7 nm between the central bright spots and the adjacent bright spots, correlating well with the calculated Pc-to-HBC distance (see Figure 4). A separation of 3.3 nm for the two outer bright spots also correlates well with the calculated edge-to-edge distance between the two HBC ligands. An apparent height of ~0.25 nm for structures of **2** is similar to that observed for structures of **1**, although again we are cautious in drawing strong conclusions from height data obtained from STM experiments. It is apparent, however, that combining two types of discotic units, HBC and phthalocyanine, leads to a dramatically modified surface structure compared to that of the HBC ligand alone.

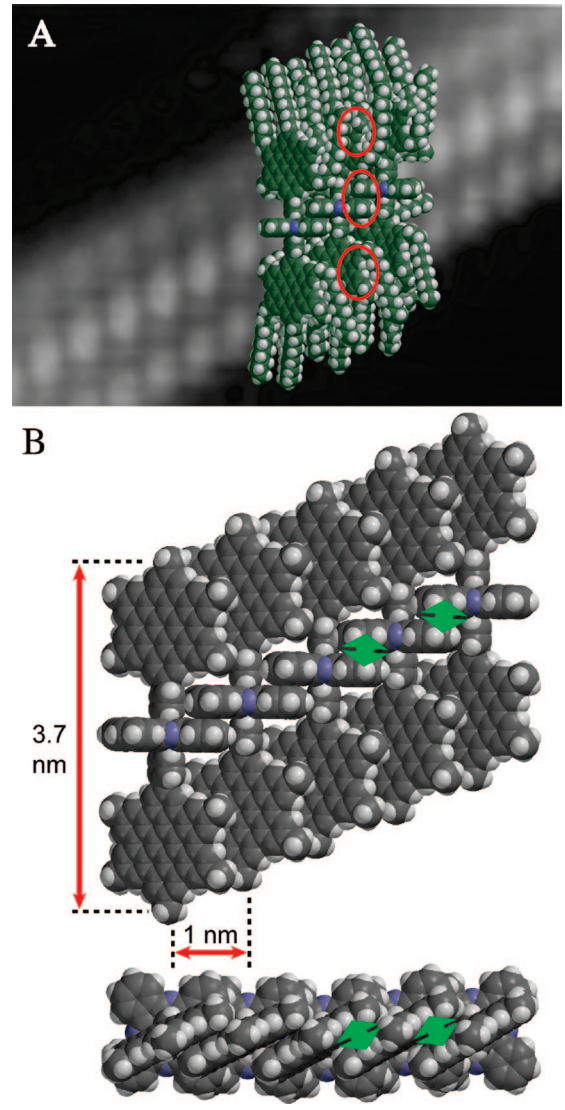

Figure 5. Packing arrangement of 2, consistent with the experimental data. (A) Magnified STM image overlaid with packing of three molecules. The red circles indicate the positions of the underlying current peak maxima. (B) Packing detail of the discotic units of 2 (C_2–C_{12} of the dodecyl chains omitted for clarity). The green arrows highlight important supramolecular interactions within the row.

In the absence of significant aryl–graphite π–π interactions involving the discotic units, CH_2–graphite interactions between alkyl chains and the graphite substrate are likely to be a driver of monolayer formation by adsorption to graphite.[28,29] Several *intra-row* supramolecular interactions that may drive the self-assembly process have been identified in our 2D packing model (Figure 5B, green arrows): π–π stacking between offset Pc units,[30] π–π stacking between HBC units, and interdigitation of dodecyl chains from adjacent molecules. The alignment of the HBC($C_{12}H_{25}$)$_5$ discotic

units, relative to the surface, is restricted by the bulky orthogonal RuPc unit and is intermediate between that of the face-on monolayer organization observed for $HBC(C_{12}H_{25})_5$ and $HBC(C_{12}H_{25})_6$ in solution at HOPG surfaces[16] and the edge-on packing of $HBC(C_{12}H_{25})_6$ in zone-cast films on treated silica.[7] In the former, HBC−surface π−π interactions dominate over HBC−HBC π−π interactions, whereas in the latter the reverse is true.

CONCLUSION

We have synthesized a new HBC compound bearing a pyridine group and a new coordination complex of this ligand. STM experiments show that the ligand and complex both form self-assembled structures on HOPG. The HBC-pyridine ligand does not appear to lie flat on the graphite surface nor form edge-on columnar structures, but rather a canted orientation with respect to the HOPG surface is indicated. STM experiments show that the HBC-py RuPc complex forms long row-like structures on HOPG. There is good correlation between the dimensions of the calculated molecular structure and the features observed in STM images. We propose that the metallophthalocyanine unit sits edge-on to the surface and the HBC ligands adopt canted orientations.

EXPERIMENTAL SECTION

General. 2-Bromo-5,8,11,14,17,-pentadodecyl - hexa-*peri*-hexabenzocoronene and $[PcRu(PhCN)_2]$ were prepared by literature procedures.[16,20] Pyridine-4-boronic acid, pinacol ester (Boron Molecular), tetrakis(triphenylphosphine)palladium(0) (Alfa Aesar), and potassium carbonate (Ajax) were obtained commercially and used as received. ^{1}H NMR spectra were recorded using a Bruker Avance DRX instrument operating at 400 MHz and are referenced to residual protonated solvent. MALDI-TOF mass spectra were recorded using a Micromass TofSpec2E instrument with a 337 nm nitrogen laser, using 7,7,8,8-tetracyanoquinodimethane as matrix, and are reported in the form *m/z* (assignment, relative intensity). UV–visible spectra were recorded in a quartz cell on a Cary 4E spectrophotometer, as chloroform (900–250 nm) or carbon disulfide (900–380 nm) solutions (we note that **2** is practically insoluble in $CHCl_3$); results are reported in the form λ (ϵ).

Synthesis of 1. A mixture of 2-bromo-5,8,11,14,17,-pentadodecylhexa-*peri*-hexabenzocoronene (200 mg, 0.139 mmol), pyridine-4-pinacol boronic ester (60 mg, 0.29 mmol), potassium carbonate (282 mg, 2.0 mol), 1-hexanol (0.5 mL), toluene (10 mL), and water (6 mL) was placed in a Schlenk tube and deoxygenated by purging with argon. Tetrakis(triphenylphosphine)palladium(0) (16 mg, 14 μmol) was added, and the mixture was heated at 80 °C with rapid stirring for 20 h, followed by cooling to room temperature. Dichloromethane (60 mL) was added, and the organic phase was washed with aqueous potassium carbonate and water, dried over magnesium sulfate, and filtered. The filtrate was taken to dryness and purified by silica gel column chromatography (dichloromethane/ethyl acetate/triethylamine (3%)) to afford **1** (136 mg, 0.094 mmol, 68%) as a yellow powder. ^{1}H NMR (3×10^{-3} M in $CDCl_3$, 325 K): δ 8.85 (d, J = 4.4 Hz, 2H), 8.28 (s, 2H), 8.23 (s, 2H), 8.15 (s, 2H), 8.06 (s, 2H), 7.95 (s, 2H), 7.82 (s, 2H), 7.57 (d, J = 4.4 Hz, 2H), 3.03, 2.98 (t, J = 7.8 Hz, 6H), 2.74 (t, J = 7.6 Hz, 4H), 1.99 (m, 6H), 1.84 (qt, J = 7.6 Hz, 4H), 1.75–1.24 (m, 90H), 0.90 (m, 15H). MS (MALDI-TOF): 1442.0 ($[M]^+$, 100), calcd for $C_{107}H_{141}N$, 1441.1. UV–vis ($CHCl_3$, 7.6×10^{-6} M): 275sh (30 000), 316sh (16 700), 332sh (27 400), 350 (61 400), 365 nm (118 800), 395 (42 000), 407sh (23 300), 443 (3500), 449 (3040), 470 (1560) nm (L mol^{-1} cm^{-1}).

Synthesis of 2. $[PcRu(PhCN)_2]$ (9.6 mg, 11.7 μmol) and **1** (35.1 mg, 24.4 μmol) were added to dichloromethane (10 mL), and the mixture was heated at gentle reflux for 18 h under an argon atmosphere. The solution was cooled to room temperture, and methanol (10 mL) was added to precipitate the product as a flocculent green solid. The crude material was collected by filtration and purified by silica gel column chromatography ($CHCl_3$/CS_2 1:1), with the product eluting first as a green band. After removal of the solvent, 26.4 mg (7.6 μmol, 65%) of a dark green powder was obtained. ^{1}H NMR (3×10^{-4} M in CS_2/$CDCl_3$ 7:3, 300 K): δ 9.32 (m, 8H), 8.57 (s, 8H), 8.51 (s, 4H), 8.47 (s, 4H), 8.13 (s, 4H), 8.07 (s, 4H), 8.02 (m, 8H), 6.02 (d, J = 6 Hz, 4H), 3.04 (m, 12H), 2.91 (d, J = 6 Hz, 4H), 2.77 (br m, 8H), 1.93 (br m, 12H), 1.75 (br m, 8H), 1.55 (qt, J = 5.2 Hz, 12 H), 1.47 (qt, J = 6.5 Hz, 8H), 1.43–1.20 (m, 160H), 0.96 (t, J = 6.8 Hz, 12H), 0.89 (m, 18H). MS (MALDI-TOF): 1440.8 ($[\mathbf{1}]^+$, 100), calcd 1441.1; $[M]^+$ is not observed. UV–vis ($CHCl_3$, 3.2×10^{-6} M): 325 (125 400), 368 (127 100), 444 (76 700), 460sh (68 600), 573sh (27 600), 640 (60 000) nm (L mol^{-1} cm^{-1}). UV–vis (CS_2, 5.5×10^{-6} M): 406sh (100 000), 460 (41 600), 576 (25 500), 633 (67 200) nm (L mol^{-1} cm^{-1}).

STM Experiments. The STM studies were carried out with a Nanosurf EasyScan system under ambient conditions. STM tips were prepared from Pt/Ir wire (80%/20%), mechanically cut under ambient conditions. Samples were prepared by applying a toluene solution (1 mmol L^{-1}) of **1** or **2** onto a HOPG substrate. STM piezoelectric scanners were calibrated laterally with graphite (0001). All images were acquired in a constant current mode. Typical imaging conditions are bias voltages of −0.2 to −1 V (negative bias voltages indicate the STM tip is negative with respect to the substrate) and a tunnelling current of 3 pA to 1 nA.

Molecular Modeling. Equilibrium geometry optimization was achieved using the molecular mechanics method (MMFF94 force fields) within the Spartan[24] program. A range of strategically chosen starting conformations involving the RuPc, pyridine, and $HBC(R)_5$ (R = H, Me) units were minimized to determine equilibrium geometry energy minima of the discotic components. Assemblies of 2–5 $RuPc\{HBC(Me)_5\text{-}4\text{-}py\}_2$ molecules were also minimized using molecular mechanics to determine the most likely packing arrangements and identify significant intermolecular supramolecular interactions (molecule−substrate interactions were not included in the models). The dodecyl chains of **2** were added manually to best reflect the packing observed within the STM images.

Acknowledgment. The authors thank the Australian Research Council for financial support. A.M.M. and N.T.L. hold ARC Australian Postdoctoral Fellowships.

Supporting Information Available: STM images of larger area scans, STM images acquired at different scan rates, and synthetic procedures. This material is available free of charge *via* the Internet at http://pubs.acs.org.

REFERENCES AND NOTES

1. Chandrasekar, S. Discotic Liquid Crystals A Brief Review. *Liq. Cryst.* **1993**, *14*, 3–14.
2. Bushby, R. J.; Lozman, O. R. Discotic Liquid Crystals 25 Years On. *Curr. Opin. Colloid Interface Sci.* **2002**, *7*, 343–354.
3. van der Craats, A. M.; Warman, J. M. The Core-Size Effect on the Mobility of Charge in Discotic Liquid Crystalline Materials. *Adv. Mater.* **2001**, *13*, 130–133.
4. Warman, J. M.; van der Craats, A. M. Charge Mobility In Discotic Materials Studied By PR-TRMC. *Mol. Cryst. Liq. Cryst.* **2003**, *396*, 41–72.

5. Schmidt-Mende, L.; Fechtenkötter, A.; Müllen, K.; Moons, E.; Friend, R. H.; MacKenzie, J. D. Self-organized discotic liquid crystals for high-efficiency organic photovoltaics. *Science* **2001**, *293*, 1119–1122.
6. Mori, T.; Takeuchi, H.; Fujikawa, H. Field-effect Transistors Based on a Polycyclic Aromatic Hydrocarbon Core as a Two-dimensional Conductor. *J. Appl. Phys.* **2005**, *97*, 066102/1066102/3.
7. Pisula, W.; Menon, A.; Stepputat, M.; Lieberwirth, I.; Kolb, U.; Tracz, A.; Sirringhaus, H.; Pakula, T.; Müllen, K. A Zone-Casting Technique for Device Fabrication of Field Effect Transistors Based On Discotic Hexa-peri-hexabenzocoronene. *Adv. Mater.* **2005**, *17*, 684–689.
8. Tracz, A.; Jeszka, J. K.; Watson, M. D.; Pisula, W.; Müllen, K.; Pakula, T. Uniaxial Alignment of the Columnar Super-Structure of a Hexa(alkyl)hexa-peri-hexabenzocoronene on Untreated Glass by Simple Solution Processing. *J. Am. Chem. Soc.* **2003**, *125*, 1682–1683.
9. El Hamaoui, B.; Laquai, F.; Baluschev, S.; Wu, J.; Müllen, K. A phosphorescent hexa-*peri*-hexabenzocoronene platinum complex and its time-resolved spectroscopy. *Synth. Met.* **2006**, *156*, 1182–1186.
10. Kim, K.-Y.; Liu, S.; Köse, M. E.; Schanze, K. S. Photophysics of Platinum-Acetylide Substituted Hexa-peri-hexabenzocoronenes. *Inorg. Chem.* **2006**, *45*, 2509–2519.
11. Wu, J.; El Hamaoui, B.; Li, J.; Zhi, L.; Kolb, U.; Müllen, K. Solid-State Synthesis of "Bamboo-Like" and Straight Carbon Nanotubes by Thermolysis of Hexa-peri-hexabenzocoronene–Cobalt Complexes. *Small* **2005**, *1*, 210–212.
12. Herwig, P. T.; Enkelmann, V.; Schmelz, O.; Müllen, K. Synthesis and Structural Characterization of Hexa-tert-butyl-hexa-peri-hexabenzocoronene, Its Radical Cation Salt and Its Tricarbonylchromium Complex. *Chem. Eur. J.* **2000**, *6*, 1834–1839.
13. El Hamaoui, B.; Zhi, L.; Wu, J.; Li, J.; Lucas, N. T.; Tomović, Z.; Kolb, U.; Müllen, K. Solid-State Pyrolysis of Polyphenylene–Metal Complexes: A Facile Approach Toward Carbon Nanoparticles. *Adv. Funct. Mater.* **2007**, *17*, 1179–1187.
14. Wu, J.; Pisula, W.; Müllen, K. Graphenes as Potential Material for Electronics. *Chem. Rev.* **2007**, *107*, 718–747.
15. Miyaura, N.; Suzuki, A. Palladium-Catalyzed Cross-Coupling Reactions of Organoboron Compounds. *Chem. Rev.* **1995**, *95*, 2457–2483.
16. Ito, S.; Wehmeier, M.; Brand, J. D.; Kübel, C.; Epsch, R.; Rabe, J. P.; Müllen, K. Synthesis and Self-Assembly of Functionalized Hexa-*peri*-hexabenzocoronenes. *Chem. Eur. J.* **2000**, *6*, 4327–4342.
17. Clar, E. *The Aromatic Sextet*; John Wiley & Sons: London, 1972.
18. Kastler, M.; Schmidt, J.; Pisula, W.; Sebastiani, D.; Müllen, K. From Armchair to Zigzag Peripheries in Nanographenes. *J. Am. Chem. Soc.* **2006**, *128*, 9526–9534.
19. Stabel, A.; Herwig, P.; Müllen, K.; Rabe, J. P. Diodelike Current−Voltage Curves for a Single Molecule-Tunneling Spectroscopy with Submolecular Resolution of an Alkylated, *peri*-Condensed Hexabenzocoronene. *Angew. Chem., Int. Ed.* **1995**, *34*, 1609–1611.
20. Bossard, G. E.; Abrams, M. J.; Darkes, M. C.; Vollano, J. F.; Brooks, R. C. Convenient Synthesis of Water Soluble, Isomerically Pure Ruthenium Phthalocyanine Complexes. *Inorg. Chem.* **1995**, *34*, 1524–1527.
21. Hanack, M.; Polley, R. Synthesis of (2,3-Naphthalocyaninato)ruthenium(II) and Reactions with Bidentate Ligands. *Inorg. Chem.* **1994**, *33*, 3201–3204.
22. Rawling, T.; McDonagh, A. Ruthenium phthalocyanine and naphthalocyanine complexes: Synthesis, properties and applications. *Coord. Chem. Rev.* **2007**, *251*, 1128–1157.
23. Fischbach, I.; Pakula, T.; Minkin, P.; Fechtenkötter, A.; Müllen, K.; Spiess, H. W.; Saalwächter, K. Structure and Dynamics in Columnar Discotic Materials: A Combined X-ray and Solid-State NMR Study of Hexabenzocoronene Derivatives. *J. Phys. Chem. B* **2002**, *106*, 6408–6418.
24. *Spartan '04*; Wavefunction, Inc.: Irvine, CA, 2004.
25. Bumm, L. A.; Arnold, J. J.; Dunbar, T. D.; Allara, D. L.; Weiss, P. S. Electron Transfer through Organic Molecules. *J. Phys. Chem. B* **1999**, *103*, 8122–8127.
26. *SPIP Scanning Probe Image Processor*, Version 2.1; Image Metrology ApS: Lyngby, Denmark.
27. Yang, X.; Kritikos, M.; Akermark, B.; Sun, L. Axial ligand exchange reaction on ruthenium phthalocyanines. *J. Porphyrins Phthalocyanines* **2005**, *9*, 248–255.
28. Hermann, B. A.; Scherer, L. J.; Housecroft, C. E.; Constable, E. C. Self-Organized Monolayers: A Route to Conformational Switching and Read-Out of Functional Supramolecular Assemblies by Scanning Probe Methods. *Adv. Funct. Mater.* **2005**, *16*, 211–235.
29. Yin, S.; Wang, C.; Qiu, X.; Xu, B.; Bai, C. Theoretical study of the effects of intermolecular interactions in self-assembled long-chain alkanes adsorbed on graphite surface. *Surf. Interface Anal.* **2001**, *32*, 248–252.
30. de la Torre, G.; Claessens, C. G.; Torres, T. Phthalocyanines: old dyes, new materials. Putting color in nanotechnology. *Chem. Commun.* **2007**, 2000–2015.